

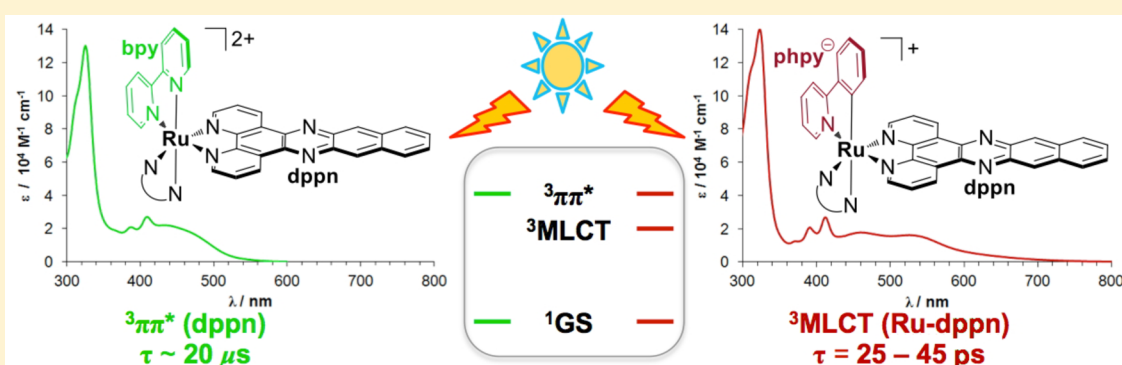
Excited State Dynamics of Two New Ru(II) Cyclometallated Dyes: Relation to Cells for Solar Energy Conversion and Comparison to Conventional Systems

Bruno Peña,[†] Nicholas A. Leed,[‡] Kim R. Dunbar,^{*,†} and Claudia Turro^{*,‡}

[†]Department of Chemistry, Texas A&M University, College Station, Texas 77840, United States

[‡]Department of Chemistry and Biochemistry, The Ohio State University, Columbus, Ohio 43210, United States

Supporting Information



ABSTRACT: The preparation, characterization, and photophysical properties of a series of ruthenium(II) complexes possessing the cyclometallating deprotonated 2-phenyl pyridine ligand, phpy^- , together with dppn (benzo[*i*]dipyrido[3,2-*a*:2',3'-*c*]phenazine), a ligand with an extended π -system, are reported. Related complexes have been used as efficient dyes in dye-sensitized solar cells (DSSCs), and the $\text{Ru} \rightarrow \text{dppn}$ metal-to-ligand charge transfer (MLCT) absorption of the new complexes $[\text{Ru}(\text{phpy})(\text{bpy})(\text{dppn})]^+$ (4) and $[\text{Ru}(\text{phpy})(\text{dppn})_2]^+$ (5) is red-shifted relative to the $\text{Ru} \rightarrow \text{bpy}$ MLCT peak in $[\text{Ru}(\text{phpy})(\text{bpy})_2]^+$ (3). These new compounds are compared to conventional complexes where phpy^- is replaced by 2,2'-bipyridine (bpy), including $[\text{Ru}(\text{bpy})_3]^{2+}$, $[\text{Ru}(\text{bpy})_2(\text{dppn})]^{2+}$ (1), and $[\text{Ru}(\text{bpy})(\text{dppn})_2]^{2+}$ (2). Unlike 1 and 2, with long-lived dppn-centered $^3\pi\pi^*$ excited states ($\tau \sim 20 \mu\text{s}$), the corresponding cyclometallated complexes 4 and 5 exhibit weakly emissive $\text{Ru} \rightarrow \text{dppn}$ $^3\text{MLCT}$ states with transient absorption lifetimes of 25 and 45 ps, respectively, which are significantly shorter than that of 3, $\sim 9 \text{ ns}$. Although it is desirable to shift the absorption of ruthenium dyes used in DSSCs to lower energies, it is evident from this work, that for cyclometallated phpy^- complexes, lowering the energy of the $^3\text{MLCT}$ state below that of 3 results in significant shortening of the excited state lifetime. The fast excited state decay, together with the lower energy of the $^1\text{MLCT}$ state, may result in lower charge injection efficiencies from these types of complexes.

INTRODUCTION

Cyclometallated complexes of ruthenium(II) have recently been shown to act as efficient dyes in dye-sensitized solar cells (DSSCs).^{1–10} Although the related complexes of Ir(III) are highly emissive and potentially useful for use in light emitting devices,^{11–13} those of Ru(II) are only weakly luminescent, and their excited state lifetimes are significantly shorter than those of related ruthenium dyes with polypyridyl ligands.^{1–6} In spite of the short lifetimes of these complexes, they are useful because charge injection from the excited state of the ruthenium dyes into semiconductor electrodes can take place on the ultrafast timescale and represents the first step after photon absorption in DSSCs.^{14–21} Because the electron injection is fast, it is important to understand the dynamics that follow vertical excitation into the Franck–Condon singlet excited state and the excited state redox properties of the dye.^{22,23}

There is evidence that a significant fraction of electron injection from the N3 and related Ru(II) dyes into TiO_2 takes place from the singlet metal-to-ligand charge transfer ($^1\text{MLCT}$) excited state, such that population of the $^3\text{MLCT}$ state competes with the charge transfer process.^{22–26} Similar results were recently reported for the ultrafast ligand dissociation in Ru(II) complexes, which is thought to take place from the singlet manifold within $\leq 1 \text{ ps}$.²⁷ It is apparent that the rate of charge injection in the dyes must be very fast, since it competes with intersystem crossing, which was measured to be $40 \pm 15 \text{ fs}$ in $[\text{Ru}(\text{bpy})_3]^{2+}$ (bpy = 2,2'-bipyridine) in one fluorescence upconversion study,^{28,29} and $15 \pm 10 \text{ fs}$ in another.³⁰ Femtosecond stimulated Raman measurements resulted in

Received: June 27, 2012

Revised: September 28, 2012

Published: September 28, 2012

the formation of the vibrations of the $^3\text{MLCT}$ within 110 fs, and led to an upper limit for the $^1\text{MLCT}$ state lifetime at <30 fs.³¹ It is believed that charge injection from the $^1\text{MLCT}$ is faster than that from the $^3\text{MLCT}$ state because of the significantly greater driving force for the charge transfer process from the former compared to the latter.^{16,17,24–26}

The control of the energies and dynamics of the excited state manifolds of Ru(II) complexes is important to improve their photochemical properties and can be achieved by varying the ligation sphere. In one key example, $[\text{Ru}(\text{bpy})_2(\text{dppn})]^{2+}$ (**1**, $\text{dppn} = \text{benzo}[i]\text{dipyrido}[3,2-a:2',3'-c]\text{phenazine}$, Figure 1) was

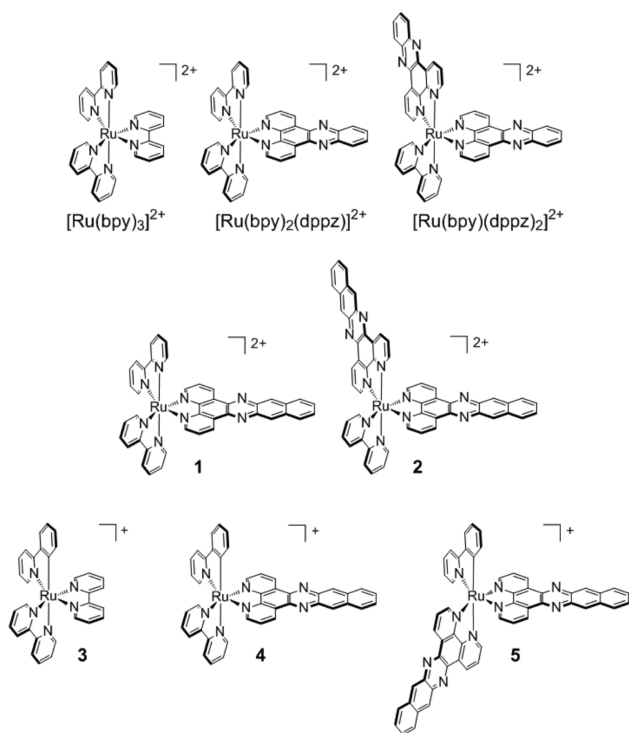


Figure 1. Schematic representation of the molecular structures of Ru(II) complexes.

shown to possess a lowest-lying excited state that is $^3\pi\pi^*$ in nature and centered on the dppn ligand with a lifetime of 33 μs .³² In this system, the dppn $^3\pi\pi^*$ state is lower in energy than the $\text{Ru} \rightarrow \text{bpy}$ and $\text{Ru} \rightarrow \text{dppn}$ $^3\text{MLCT}$ states, and is believed to lie at ~ 1.5 eV above the ground state. It should be noted, however, that the excited state ordering is reversed in the singlet manifold, where the $^1\text{MLCT}$ state lies below the dppn $^1\pi\pi^*$ state, with absorption maxima at 444 and 411 nm, respectively.³² These results clearly support the contention that inspection of the absorption spectra does not always provide the necessary information on the reactive triplet excited states of ruthenium(II) complexes. Similar findings were also reported for ruthenium complexes possessing tridentate ligands.^{33,34}

Although cyclometallated ruthenium systems have been used successfully in DSSCs, their excited state properties at early times after excitation remain to be investigated in detail. It is known that for Ru(II) complexes possessing tridentate cyclometallated ligands, the emission lifetime is ~ 125 -fold shorter than for corresponding compounds where the ligand is coordinated through a nitrogen atom.³ Similarly short emission lifetimes were reported for $\text{cis-}[\text{Ru}(\text{CH}_3\text{CN})_2(\text{bpy})(\text{phpy})]^+$ ($\text{phpy}^- = 2\text{-phenylpyridine deprotonated at the } 2'\text{-position}$)

and $[\text{Ru}(\text{dcbpy})(\text{bpy})(\text{phpy})]^+$ ($\text{dcbpy} = 2,2'\text{-bipyridine-4,4'-dicarboxylic acid}$), 10.7 and 9.3 ns, respectively.⁴ In addition, transient absorption spectroscopy on bimetallic ruthenium complexes with tridentate cyclometallating ligands appeared in the literature.³⁵ In this work, the lifetime of $[\text{Ru}(\text{tpy})(\text{L})]^+$, where $\text{tpy} = 2,2':6',2''\text{-terpyridine}$ and L represents the cyclometallating ligand 4-(4-bromophenyl)-6-phenyl-2,2'-bipyridine deprotonated at the *ortho* position of the phenyl ring, was reported to be >1 ns from transient absorption measurements.³⁵ To our knowledge, these represent the only reports of ultrafast transient absorption spectroscopy on cyclometallated complexes of ruthenium.

The present work focuses on the investigation of two new cyclometallated complexes and on the comparison of their photophysical properties to those of the analogous bpy systems. The complexes in the series also include the dppz (dipyrido-[3,2-*a*:2',3'-*c*]phenazine) and dppn ligands to further probe the relative energies of the MLCT and $\pi\pi^*$ excited states. These ligands are of interest because ruthenium(II) complexes with low-lying π^* orbitals were recently reported as efficient sensitizers of TiO_2 at low wavelengths.³⁶ Specifically, the complexes $[\text{Ru}(\text{bpy})(\text{dppz})_2][\text{PF}_6]_2$, $[\text{Ru}(\text{bpy})_2(\text{dppn})][\text{PF}_6]_2$ (**1**), $[\text{Ru}(\text{bpy})(\text{dppn})_2][\text{PF}_6]_2$ (**2**), $[\text{Ru}(\text{phpy})(\text{bpy})_2][\text{PF}_6]_2$ (**3**), $[\text{Ru}(\text{phpy})(\text{bpy})(\text{dppn})][\text{PF}_6]$ (**4**), and $[\text{Ru}(\text{phpy})(\text{dppn})_2][\text{PF}_6]$ (**5**) were prepared, and their excited state dynamics were investigated and compared. The molecular structures of compounds **1–5** and related Ru(II) complexes are depicted in Figure 1. The results of this study are important in the context of designing new systems and, importantly, they reveal that the inclusion of the phpy^- ligand in the coordination sphere significantly lowers the energy of the MLCT excited states and reduces their lifetime.

EXPERIMENTAL SECTION

Materials. The solvents used were of reagent grade quality. Ethanol (KORTEP, 200 proof) was dried over Mg/I_2 and distilled prior to use. Normal butanol (Mallinckrodt), acetonitrile (EMD Chemicals) and toluene (EMD Chemicals) were used as received without further purification. Standard Schlenk-line techniques (dry N_2 atmosphere) were used to maintain anaerobic conditions during preparation of the compounds. Analytical thin layer chromatography (TLC) was performed on aluminum-backed sheets coated with silica 60 F254 adsorbent (0.20 mm thickness, EMD Chemicals). Flash chromatography was carried out with silica gel 60 (230–400 mesh ASTM) from Fluka. The metal starting material $\text{RuCl}_3 \cdot 3\text{H}_2\text{O}$ was purchased from Pressure Chemicals Co., and 2,2'-bipyridine and 2-phenyl pyridine were purchased from Alfa Aesar. The compounds $[\text{Ru}(\text{bpy})(\text{NCCH}_3)_4][\text{PF}_6]_2$,³⁷ $[\text{Ru}(\text{phpy})(\text{NCCH}_3)_4][\text{PF}_6]_2$,³⁸ $\text{cis-}[\text{Ru}(\text{phpy})(\text{bpy})(\text{NCCH}_3)_2][\text{PF}_6]_2$,³⁹ $[\text{Ru}(\text{phpy})(\text{bpy})_2][\text{PF}_6]_2$ (**3**),⁶ dipyrido-[3,2-*a*:2',3'-*c*]phenazine (dppz),⁴⁰ and benzo[*i*]dipyrido[3,2-*a*:2',3'-*c*]phenazine (dppn)^{40,41} were prepared according to published procedures. The labeling scheme and the corresponding ^1H NMR spectra of $[\text{Ru}(\text{bpy})(\text{dppz})_2]^{2+}$, **2**, **4**, and **5** are depicted in Figures S1 and S2 in the Supporting Information. In the case of compound **5**, the proton resonances for each dppn ligand (24 protons overall) could not be assigned unambiguously.

$[\text{Ru}(\text{bpy})(\text{dppn})_2][\text{PF}_6]_2$ (2**).** A suspension of $[\text{Ru}(\text{bpy})(\text{NCCH}_3)_4][\text{PF}_6]_2$ (100.0 mg, 0.14 mmol) and dppn (94.3 mg, 0.28 mmol) in *n*-BuOH (15 mL) was heated to reflux for 18 h. The resulting orange precipitate was removed by filtration,

washed with diethyl ether (25 mL), and purified by column chromatography (SiO_2 , CH_3CN /toluene, gradient from 10% to 50% CH_3CN). The second intense orange band was collected and the volume was reduced to ca. 10 mL. The bright red-orange solid that precipitated was collected by filtration and washed with diethyl ether (15 mL). Yield: 96.5 mg (56%). ^1H NMR (500 MHz, $(\text{CD}_3)_2\text{CO}$): δ 9.79 (dd, 2H, $^3J = 8.0$ Hz, $^4J = 1.0$ Hz, H-c), 9.70 (dd, 2H, $^3J = 7.5$ Hz, $^4J = 1.5$ Hz, H-c'), 9.19 (s, 2H, H-d), 9.15 (s, 2H, H-d'), 8.92 (d, 2H, $^3J = 8.0$ Hz, H-4), 8.66 (dd, 2H, $^3J = 5.5$ Hz, $^4J = 1.0$ Hz, H-a), 8.62 (dd, 2H, $^3J = 5.5$ Hz, $^4J = 1.0$ Hz, H-a'), 8.42 (m, 4H, H-f, H-f'), 8.32 (d, 2H, $^3J = 5.0$ Hz, H-1), 8.26 (ddd, 2H, $^3J = 8.0$ Hz, $^3J = 8.0$ Hz, $^4J = 1.5$ Hz, H-3), 8.15 (dd, 2H, $^3J = 8.0$ Hz, $^3J = 5.5$ Hz, H-b), 7.95 (dd, 2H, $^3J = 8.0$ Hz, $^3J = 5.5$ Hz, H-b'), 7.78 (m, 4H, H-e, H-e'), 7.54 (ddd, 2H, $^3J = 7.5$ Hz, $^3J = 5.5$ Hz, $^4J = 1.5$ Hz, H-2). HRMS (ESI⁺): Calcd. for $[\text{C}_{54}\text{H}_{32}\text{N}_{10}\text{Ru}]^{2+}$ ($[\text{M}-2\text{PF}_6]^{2+}$), 461.0928. Found: 461.0948. Anal. Calcd. for $\text{C}_{54}\text{H}_{32}\text{F}_{12}\text{N}_{10}\text{P}_2\text{Ru}\cdot 9.75\text{H}_2\text{O}$: C, 46.74; H, 3.74; N, 10.09. Found: C, 45.37; H, 2.37; N, 9.82.

[Ru(bpy)(dppz)₂][PF₆]₂. A suspension of $[\text{Ru}(\text{bpy})(\text{NCCH}_3)_4][\text{PF}_6]_2$ (162.5 mg, 0.23 mmol) and dppz (129.8 mg, 0.46 mmol) in *n*-BuOH (15 mL) was heated to reflux for 24 h. The resulting orange precipitate was collected by filtration, washed with diethyl ether (25 mL), and purified by column chromatography (SiO_2 , CH_3CN /toluene, gradient from 10% to 30% CH_3CN). The first intense orange band was collected and reduced to dryness to give a bright red-orange solid. Yield: 129.2 mg (60%). ^1H NMR (500 MHz, $(\text{CD}_3)_2\text{CO}$): δ 9.81 (dd, 2H, $^3J = 8.5$ Hz, $^4J = 1.5$ Hz, H-c), 9.72 (dd, 2H, $^3J = 8.5$ Hz, $^4J = 1.5$ Hz, H-c'), 8.90 (d, 2H, $^3J = 8.0$ Hz, H-4), 8.68 (dd, 2H, $^3J = 5.5$ Hz, $^4J = 1.5$ Hz, H-a), 8.59 (dd, 2H, $^3J = 5.5$ Hz, $^4J = 1.0$ Hz, H-a'), 8.54–8.48 (m, 4H, H-e, H-e'), 8.25 (m, 4H, H-1, H-3), 8.21 (m, 4H, H-d, H-d'), 8.16 (dd, 2H, $^3J = 8.5$ Hz, $^3J = 5.5$ Hz, H-b), 7.93 (dd, 2H, $^3J = 8.5$ Hz, $^3J = 5.5$ Hz, H-b'), 7.50 (ddd, 2H, $^3J = 7.5$ Hz, $^3J = 5.5$ Hz, $^4J = 1.5$ Hz, H-2). HRMS (ESI⁺): Calcd. for $[\text{C}_{46}\text{H}_{28}\text{N}_{10}\text{Ru}]^{2+}$ ($[\text{M}-2\text{PF}_6]^{2+}$), 411.0771. Found: 411.0760. Anal. Calcd. for $\text{C}_{46}\text{H}_{28}\text{F}_{12}\text{N}_{10}\text{P}_2\text{Ru}\cdot 4\text{H}_2\text{O}$: C, 46.67; H, 3.07; N, 11.83. Found: C, 46.07; H, 2.35; N, 11.79.

[Ru(phpp)(bpy)(dppn)][PF₆]₂ (4). A dark brown suspension of *cis*- $[\text{Ru}(\text{phpp})(\text{bpy})(\text{NCCH}_3)_2][\text{PF}_6]_2$ (155.1 mg, 0.24 mmol) and dppn (81.2 mg, 0.24 mmol) in EtOH (20 mL) was heated to reflux under reduced light conditions. The solution became dark red in color within 5 min. After 8 h, the dark red solution was reduced to dryness, and the solid residue was purified by column chromatography (SiO_2 , CH_3CN /toluene, gradient from 10% to 30% CH_3CN). The second red band was collected and the volume was reduced to ca. 15 mL. The dark red solid that precipitated from solution was collected by filtration and washed with diethyl ether (25 mL). Yield: 96.8 mg (45%). ^1H NMR (500 MHz, $(\text{CD}_3)_2\text{CO}$): δ 9.50 (dd, 1H, $^3J = 8.0$ Hz, $^4J = 1.5$ Hz, H-c or H-c'), 9.31 (dd, 1H, $^3J = 8.0$ Hz, $^4J = 1.5$ Hz, H-c' or H-c), 8.97 (s, 1H, H-d or H-d'), 8.96 (s, 1H, H-d' or H-d), 8.64 (d, 2H, $^3J = 8.0$ Hz, H-4', H-5'), 8.52 (dd, 1H, $^3J = 5.5$ Hz, $^4J = 1.5$ Hz, H-a or H-a'), 8.50 (dd, 1H, $^3J = 5.5$ Hz, $^4J = 1.5$ Hz, H-a' or H-a), 8.31 (m, 2H, H-f, H-f'), 8.21 (d, 1H, $^3J = 8.0$ Hz, H-5), 8.08 (d, 1H, $^3J = 5.5$ Hz, H-1'), 8.03–7.97 (m, 5H, H-b or H-b', H-4, H-3', H-6', H-8'), 7.90 (d, 1H, $^3J = 5.5$ Hz, H-8), 7.77 (m, 2H, H-b' or H-b, H-6), 7.71 (m, 2H, H-e, H-e'), 7.45 (ddd, 1H, $^3J = 7.5$ Hz, $^3J = 5.5$ Hz, $^4J = 1.5$ Hz, H-2'), 7.29 (ddd, 1H, $^3J = 7.5$ Hz, $^3J = 5.5$ Hz, $^4J = 1.5$ Hz, H-7'), 7.00 (m, 2H, H-3, H-7), 6.91 (ddd, 1H, $^3J = 7.5$ Hz,

$^3J = 7.5$ Hz, $^4J = 1.5$ Hz, H-2), 6.61 (dd, 1H, $^3J = 7.5$ Hz, $^4J = 1.0$ Hz, H-1). HRMS (ESI⁺): Calcd. for $[\text{C}_{43}\text{H}_{28}\text{N}_7\text{Ru}]^+$ ($[\text{M}-\text{PF}_6]^+$), 744.1450. Found: 744.1457. Anal. Calcd. for $\text{C}_{43}\text{H}_{28}\text{F}_6\text{N}_7\text{PRu}\cdot 0.25\text{H}_2\text{O}$: C, 57.82; H, 3.22; N, 10.98. Found: C, 57.88; H, 3.21; N, 10.89.

[Ru(phpp)(dppn)₂][PF₆]₂ (5). A light brown suspension of $[\text{Ru}(\text{phpp})(\text{NCCH}_3)_4][\text{PF}_6]_2$ (101.0 mg, 0.18 mmol) and dppn (119.2 mg, 0.36 mmol) in EtOH (20 mL) was heated to reflux under reduced light conditions. The mixture turned to a dark brown-red solution within 5 min, and after 8 h the resulting dark red solution was reduced to dryness. The resulting solid residue was purified by column chromatography (SiO_2 , CH_3CN /toluene, gradient from 10% to 25% CH_3CN). The first red band was collected, and the volume was reduced to ca. 20 mL. The dark red solid that precipitated from solution was removed by filtration and washed with diethyl ether (25 mL). Yield: 113.1 mg (60%). ^1H NMR (500 MHz, $(\text{CD}_3)_2\text{CO}$): δ 9.53 (dd, 1H, $^3J = 8.0$ Hz, $^4J = 1.0$ Hz, H-C), 9.45 (dd, 1H, $^3J = 8.0$ Hz, $^4J = 1.0$ Hz, H-C), 9.27 (dd, 1H, $^3J = 8.0$ Hz, $^4J = 1.0$ Hz, H-C), 9.17 (dd, 1H, $^3J = 8.0$ Hz, $^4J = 1.0$ Hz, H-C), 9.07 (s, 1H, H-D), 9.01 (s, 1H, H-D), 8.98 (s, 1H, H-D), 8.83 (s, 1H, H-D), 8.68 (dd, 1H, $^3J = 5.5$ Hz, $^4J = 1.5$ Hz, H-A), 8.62 (dd, 1H, $^3J = 5.5$ Hz, $^4J = 1.5$ Hz, H-A), 8.46 (dd, 1H, $^3J = 5.5$ Hz, $^4J = 1.0$ Hz, H-A), 8.41 (dd, 1H, $^3J = 5.5$ Hz, $^4J = 1.0$ Hz, H-A), 8.39–8.28 (m, 4H, H-F), 8.22 (d, 1H, $^3J = 8.5$ Hz, H-5), 8.08 (d, 1H, $^3J = 8.0$ Hz, H-4), 8.06 (d, 1H, $^3J = 5.0$ Hz, H-8), 7.93–7.83 (m, 3H, 2 H-B, H-6), 7.76–7.66 (m, 6H, 2 H-B, 4 H-E), 7.05 (ddd, 1H, $^3J = 7.0$ Hz, $^3J = 5.5$ Hz, $^4J = 1.5$ Hz, H-7), 7.00 (ddd, 1H, $^3J = 7.5$ Hz, $^3J = 7.5$ Hz, $^4J = 1.0$ Hz, H-3), 6.92 (ddd, 1H, $^3J = 7.5$ Hz, $^3J = 7.5$ Hz, $^4J = 1.0$ Hz, H-2), 6.83 (d, 1H, $^3J = 7.5$ Hz, H-1). HRMS (ESI⁺): Calcd. for $[\text{C}_{55}\text{H}_{32}\text{N}_9\text{Ru}]^+$ ($[\text{M}-\text{PF}_6]^+$), 920.1834. Found: 920.1820. Anal. Calcd. for $\text{C}_{55}\text{H}_{32}\text{F}_6\text{N}_9\text{PRu}\cdot \text{H}_2\text{O}$: C, 61.00; H, 3.16; N, 11.64. Found: C, 60.98; H, 2.79; N, 11.59.

Instrumentation. ^1H nuclear magnetic resonance (NMR) spectra were measured on a Varian 500 MHz spectrometer. Chemical shifts (δ) are reported in parts per million (ppm) from low to high field and referenced to residual nondeuterated solvent (2.05 ppm in acetone- d_6). Standard abbreviations indicating multiplicity are used, where s = singlet, d = doublet, t = triplet, and m = multiplet. Steady-state absorption spectra were recorded on a Shimadzu UVPC-3001 spectrophotometer or a HP diode array spectrometer (HP8453) with HP8453 Win System software. Corrected steady-state emission spectra were measured on a Horiba Jobin Yvon Fluoromax-4 spectrometer. Electrochemical measurements were carried out by using an HCH Electrochemical Analyzer model CH 1620A. Electrospray mass spectra were acquired on an Applied Biosystems PE SCIEX QSTAR mass spectrometer (MDS Sciex). Elemental analyses were performed by Atlantic Microlab, Inc. (Norcross, GA).

The home-built transient absorption instrument for measurements on the nanosecond and microsecond timescales was previously reported,³⁴ using a frequency-doubled or tripled (532 or 355 nm, respectively) Spectra-Physics GCR-150 Nd:YAG laser (fwhm ~ 8 ns) as the excitation source. Femtosecond transient absorption experiments were carried out using laser and detection systems that were previously described.⁴² The samples were excited at 310 nm, 580 nm, or 595 nm (~ 1 – 2 mW at the sample) by the output of an optical parametric amplifier equipped with a sum frequency generation or ultraviolet/visible harmonics attachment. During the measurements, the irradiated volume was kept in constant

Table 1. Electronic Absorption Maxima with Intensities and Electrochemical Data for 1–5 and Related Complexes Measured in CH₃CN

complex	$\lambda_{\text{abs}}/\text{nm}$ ($\epsilon \times 10^3 \text{ M}^{-1} \text{ cm}^{-1}$)	$E_{1/2}/\text{V}^a$
[Ru(bpy) ₃] ²⁺	286 (75.5), 450 (13.0)	+1.54, −1.07, −1.26, −1.53
[Ru(bpy) ₂ (dppz)] ²⁺	284 (104), 320 (21.4), 359 (17.5), 370 (17.2), 445 (16.3) ^c	+1.57, −0.73, −1.15 ^b
[Ru(bpy)(dppz)] ²⁺	280 (110.9), 317 (26.5), 359 (25.8), 367 (24.9), 445 (15.8)	+1.62, −0.73, −1.22, −1.51
[Ru(bpy) ₂ (dppn)] ²⁺ (1)	285 (65.6), 390 (9.4), 414 (12.5), 444 (13.5) ^b	+1.58, −0.46 ^c
[Ru(bpy)(dppn)] ²⁺ (2)	285 (59.2), 325 (128.4), 387 (20.7), 409 (26.9), 444 (21.3)	+1.61, −0.50, −1.00, −1.10
[Ru(phpy)(bpy)] ²⁺ (3)	293 (46.4), 369 (8.92), 404 (8.23), 492 (6.48), 546 (7.38)	+0.72, −1.36, −1.62
[Ru(phpy)(bpy)(dppn)] ⁺ (4)	298 (69.1), 320 (74.4), 391 (16.0), 411 (18.7), 485 (12.0), 546 (11.0)	+0.76, −0.61, −1.23, −1.52
[Ru(phpy)(dppn)] ⁺ (5)	323 (143.4), 391 (20.9), 412 (27.0), 460 (17.8), 525 (16.3)	+0.80, −0.61, −1.27

^avs NHE, 0.1 M [Bu₄N][PF₆], 0.2 V/s, 298 K, Ag/AgCl (KCl_(aq) 3M) reference electrode. ^bFrom ref 48. ^cFrom ref 32.

motion by using a demountable liquid Harrick flow cell with Swagelok fittings and CaF₂ windows (1 mm thick in the front to minimize group velocity dispersion and 2 mm thick in the back). The windows were separated by 1 mm thick PTFE spacer, and the sample was pumped through the flow cell via a magnetic drive gear pump (Micropump, Inc., 415A) with a brushless pump head (GA series). A total volume of ~7 mL was required for the flow cell to operate correctly. To ensure that no photodecomposition occurred during data collection, absorption spectra were recorded before and after the transient absorption measurements. The measurement at each of the pump–probe delay positions was repeated four times to confirm data reproducibility throughout the experiment, and the resulting spectra were corrected for the chirp in the white-light continuum.⁴³

Methods. Density functional theory (DFT) calculations were performed with the Gaussian 09 package,⁴⁴ using the Becke's three-parameter hybrid functional and the Lee–Yang–Parr's gradient-corrected correlation functional (B3LYP).^{45,46} The Stuttgart RSC 1997 Electron Core Potential (ECP) basis set and effective core potential were used for the Ru atom and the split-valence 6-311G* basis set was used for the other elements. The geometry optimizations were performed using the polarized continuum medium model (PCM, acetonitrile) to include solvent polarization effects and without symmetry restraints, with subsequent frequency analysis to show that the structures are local minima on the potential energy surface. Time-dependent density functional theory (TD-DFT) calculations were performed to arrive at the vertical singlet excited states for each complex from the corresponding optimized singlet ground state geometry using the PCM model with acetonitrile as the solvent. Fragment contributions to the MOs were calculated using the Chemissian v2.2 software.⁴⁷

Cyclic voltammetric measurements were performed in CH₃CN (distilled from 3 Å molecular sieves) with 0.1 M tetra-*n*-butylammonium hexafluorophosphate, [Bu₄N][PF₆], as the supporting electrolyte. The working electrode was a BAS Pt disk electrode, the reference electrode was Ag/AgCl, and the auxiliary electrode was a Pt wire. The ferrocene/ferrocenium couple occurs at $E_{1/2} = +0.44 \text{ V}$ vs Ag/AgCl under the same experimental conditions. The photophysical studies were conducted using acetonitrile as the solvent. For femtosecond transient absorption experiments, each sample was prepared with an optical density of 0.3 to 0.5 at the excitation wavelength, whereas an optical density of 0.5 to 1.0 at the excitation wavelength was used for nanosecond experiments. Absorbance in the range of 0.05 to 0.1 at the excitation wavelength was used for steady-state luminescence and low temperature measurements (77 K) were obtained using a

quartz NMR tube placed in a Dewar with quartz windows and filled with liquid nitrogen.

RESULTS AND DISCUSSION

Synthesis and Structural Characterization. The non-cyclometallated complexes [Ru(bpy)(dppz)]²⁺ and [Ru(bpy)(dppn)]²⁺ (2) were prepared in 56% and 60% yield, respectively, by heating [Ru(bpy)(NCCH₃)₄]²⁺ with 2 equiv of the bidentate ligands dppn and dppz, respectively, in refluxing *n*-butanol (Figure 1). Solvents of lower boiling point, such as ethanol, afforded little or very slow formation of the desired products. The tris-heteroleptic cyclometallated complex [Ru(phpy)(bpy)(dppn)]⁺ (4) was synthesized in 45% yield by heating *cis*-[Ru(phpy)(bpy)(NCCH₃)₂]⁺ with 1 equivalent of dppn in refluxing ethanol, while [Ru(phpy)(dppn)]⁺ (5) was prepared in 60% yield by reacting [Ru(phpy)(NCCH₃)₄]⁺ with 2 equiv of dppn in the same solvent. Compounds 4 and 5 were obtained as dark red solids, in contrast to the bright orange color of [Ru(bpy)(dppz)]²⁺ and 2. In all cases, the compounds were purified by flash column chromatography in SiO₂ using CH₃CN/toluene mixtures as eluent.

The identities of the new complexes were verified by ESI-MS, elemental analysis, and ¹H NMR spectroscopy (Figure S2); the proton NMR signals were assigned by collecting ¹H¹H COSY spectra (Figures S3–S6). [Ru(bpy)(dppz)]²⁺ and 2 exhibit 14 and 16 proton resonances, respectively, as expected based on their C₂ symmetry (Figures S2a,b). The spectra of the two complexes are very similar, but 2 shows two additional singlets (H-d and H-d') at 9.19 and 9.15 ppm. The protons H-a and H-a' (*ortho* to the N atom, Figure S1) from the ligands with π -extended system (dppn or dppz) appear in the 8.66–8.60 ppm range and are shifted upfield by ~1.13 ppm with respect to the protons H-c and H-c' because of the proximity of the former to the π -system of the adjacent polypyridine ligand (shielding by ring current effects). A similar scenario is found for the *ortho* protons in bpy (H-1, 8.33–8.25 ppm), where they are shifted upfield by ~0.6 ppm with respect to the *para* protons (H-4). These two types of protons are also differentiated by the magnitude of their coupling constants, where $^3J_{\text{ortho}} < ^3J_{\text{para}}$.

In the case of the cyclometallated complexes 4 and 5, their ¹H NMR spectra are more complex (Figures S2c,d), exhibiting 28 and 32 resonances, respectively, as expected for their C₁ symmetric structures. The dppn protons in the vicinity of the metal center (H-a, a', b, b', c, c') for both complexes are shifted upfield (~0.1–0.6) with respect to the same protons in 2, which can be explained by their proximity to the greater electron density located on the organometallic Ru–C_{aryl} bond. In 4, the proton *ortho* to the Ru–C_{aryl} bond at 6.61 ppm (H-1)

is shifted upfield by 1.47 ppm relative to the analogous proton of the bpy ligand (H-1') within the same molecule. The same feature is observed for **5**, for which the proton H-1 is shifted upfield and observed at 6.83 ppm. The same chemical shifts for this particular type of proton have been observed in several cyclometallated Ru complexes reported by Berlinguette and co-workers, and the relatively strong shielding is explained by the high electron density along the Ru–C_{aryl} bond.^{1–6}

Electrochemistry and Electronic Spectroscopy. The electrochemical properties of the complexes were assessed by cyclic voltammetry in CH₃CN, and the observed redox couples are listed in Table 1, where they are also compared to related compounds. All complexes display a single reversible oxidation process at positive potentials vs normal hydrogen electrode (NHE), corresponding to the metal-based oxidation, as well as several quasi-reversible processes at negative potentials associated with reduction of the ligands (Figures S7–S11). The [Ru(bpy)₂L]²⁺ (L = bpy, dppz, dppn) complexes possess a reversible metal-based, Ru(III/II), oxidation process at $E_{1/2}([Ru]^{3+/2+}) = +1.54$ to $+1.58$ V vs NHE, but they differ in their ligand-based reduction potentials, $E_{1/2}([Ru]^{2+/+})$, with values associated with the ease of reduction of [Ru(bpy)₂L]²⁺ (L = bpy, dppz, dppn) that follow the trend of the ligand L dppn > dppz > bpy (Table 1).³² The $E_{1/2}([Ru]^{3+/2+})$ couples in [Ru(bpy)(dppz)₂]²⁺ and **2**, at $+1.62$ V and $+1.61$ V vs NHE, respectively, appear at slightly more positive potentials than those of the corresponding [Ru(bpy)₂(dppz)]²⁺ and **1**, respectively, observed at $+1.57$ V and $+1.58$ V vs NHE (Table 1).³² In addition, **2** exhibits a reversible dppn ligand-based reduction at -0.50 V vs NHE, whereas the dppz ligand-based reduction in [Ru(bpy)(dppz)₂]²⁺ occurs at -0.73 V vs NHE; these values are similar to those measured for **1** and [Ru(bpy)₂(dppz)]²⁺, respectively.³²

In the case of the cyclometallated complexes **3–5**, the observed Ru(III/II) couple is observed at less positive potentials, with $E_{1/2}([Ru]^{3+/2+})$ values ranging from $+0.80$ to $+0.72$ V vs NHE. Such a cathodic shift can be ascribed to the increased electron density on the metal center afforded by the covalent binding of phpy[−] to the metal compared to the coordination by bpy. Additionally, the three cyclometallated complexes exhibit several well-resolved ligand-centered reduction waves that also show a cathodic shift with respect to [Ru(bpy)₂L]²⁺ (L = bpy, dppn) and [Ru(bpy)(L)₂]²⁺ (L = dppn, dppz). The shift can be attributed to the greater π -backbonding to the pyridyl rings of the ligand L that arises from the increased electron density at the metal center provided by cyclometallating phpy[−] ligand. For example, the first bpy-based reduction in **3** is observed at $E_{1/2}([Ru]^{2+/+}) = -1.36$ V vs NHE, shifted cathodically by 0.29 V with respect to [Ru(bpy)₃]²⁺, where $E_{1/2}([Ru]^{2+/+}) = -1.07$ V vs NHE.³² Similarly, the dppn-centered reductions of **4** and **5**, for which first reduction wave appears at $E_{1/2}([Ru]^{2+/+}) = -0.61$ V vs NHE, are shifted cathodically by 0.11 – 0.15 V with respect to the first reduction waves of [Ru(bpy)_n(dppn)_{3-n}]²⁺ ($n = 1, 2$).

The absorption maxima (λ_{abs}) and molar extinction coefficients (ϵ) of **1–5** in CH₃CN are listed in Table 1, and the electronic absorption spectra of the cyclometallated complexes **3–5** (Figure 2b) are compared to related compounds possessing bpy as the ancillary ligand, displayed in Figure 2a. Complex **2** exhibits a broad ¹MLCT transition centered at 444 nm, dppn ligand-based ¹ $\pi\pi^*$ transitions at 409 , 387 , and 325 nm, and a bpy-centered ¹ $\pi\pi^*$ transition with maximum at 285 nm, which paralleled those measured for **1**.³⁵

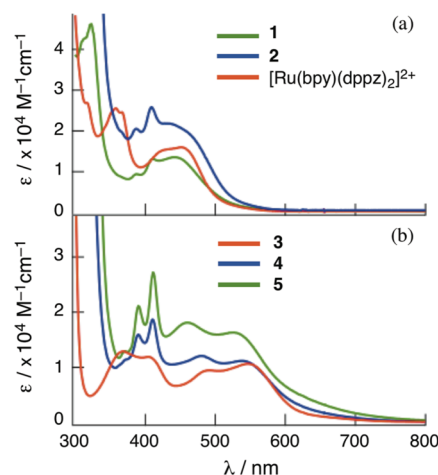


Figure 2. Electronic absorption spectra of the PF₆[−] salts of the Ru(II) complexes with (a) bpy and (b) phpy[−] as ancillary ligands in CH₃CN.

Similarly, [Ru(bpy)(dppz)₂]²⁺ displays a broad ¹MLCT transition at 445 nm, dppz ligand-based ¹ $\pi\pi^*$ transitions at 367 , 359 , and 317 nm, and a bpy ligand-based ¹ $\pi\pi^*$ transition at 280 nm; these transitions resemble those found in [Ru(bpy)₂(dppz)]²⁺ and related complexes.^{33–35,48}

The electronic absorption spectra of the cyclometallated complexes **3–5** displayed in Figure 2b differ significantly from that of [Ru(bpy)₃]²⁺ and from those of the related systems with bpy as the ancillary ligands, [Ru(bpy)_n(L)_{3-n}]²⁺ (L = dppz, dppn; $n = 1, 2$), shown in Figure 2a. In particular, **3–5** exhibit substantial bathochromic shifts of the ¹MLCT transitions relative to the corresponding bpy-containing complexes. The ¹MLCT maxima of **3**, **4** and **5** are red-shifted by 96 nm (3907 cm^{−1}), 102 nm (4207 cm^{−1}) and 81 nm (3474 cm^{−1}), with respect to [Ru(bpy)₃]²⁺, **1** and **2**, respectively. In contrast, there is little shift in the dppn-centered ¹ $\pi\pi^*$ maxima observed for the cyclometallated **4** and **5** compared to **2**, consistent with the effect of Ru-phpy[−] bonding destabilizing t_{2g}-type occupied orbitals, without significant perturbations to the energies of the π and π^* orbitals of the other ligands in the complex. The effect of cyclometallation on the energy of the highest occupied molecular orbital (HOMO) is also in agreement with the ease of oxidation of these complexes. It is also evident from Figure 2 that the ¹MLCT peaks are broader in the cyclometallated complexes (Figure 2b) as compared to the bpy-coordinated systems (Figure 2a), such that the tails of the absorption spectra of **3–5** in the visible region extend beyond 750 nm.

The ¹MLCT transitions of **3** at 492 nm ($20,325$ cm^{−1}) and 546 nm ($18,315$ cm^{−1}) have been previously assigned as Ru($4d\pi$)→bpy(π^*), while those at higher energy in the 350 – 430 nm range arise from Ru($4d\pi$)→phpy[−](π^*) transitions.⁶ Thus, the lower energy ¹MLCT bands observed for **4** and **5** between 450 and 600 nm can be assigned to Ru($4d\pi$)→bpy/dppn(π^*) transitions, whereas the transition corresponding to Ru($4d\pi$)→phpy[−](π^*) is likely obscured by the dppn ¹ $\pi\pi^*$ ligand-centered transitions in the 320 – 420 nm range. In the ultraviolet region, **3** and **4** exhibit a bpy-based ¹ $\pi\pi^*$ transition at ~ 295 nm, and **4** and **5** show dppn-centered ¹ $\pi\pi^*$ absorption maxima at ~ 410 , ~ 390 and ~ 320 nm. It should be noted that, as expected, the intensity of the dppn-centered transition at ~ 410 nm is generally commensurate with the number of dppn ligands present in the complex. For example, the intensity of the dppn-centered transitions is greater in **2**, [Ru(bpy)-

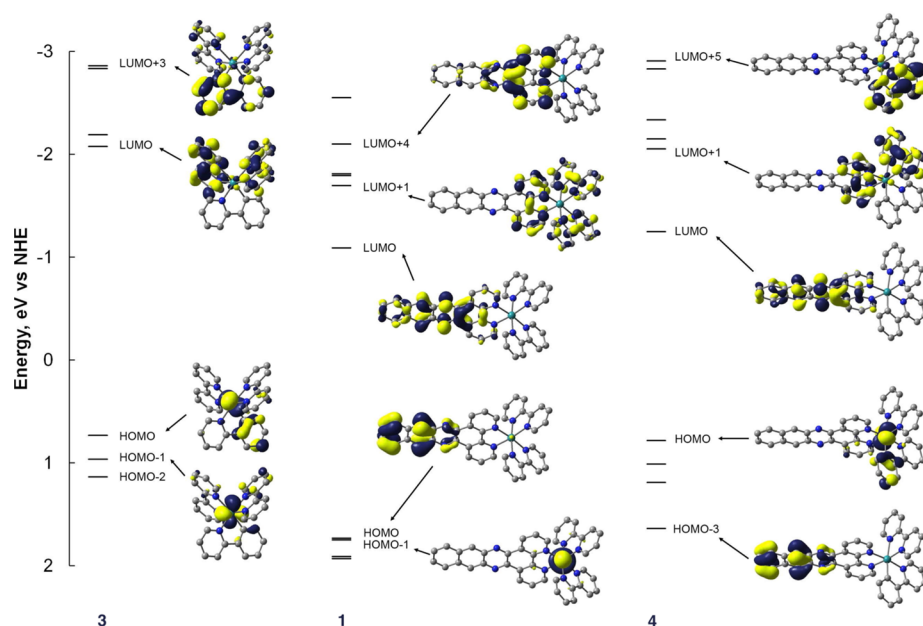


Figure 3. Molecular orbital diagrams of **3**, **1**, and **4**, and electron densities of selected MOs (isovalue = 0.04).

(dppn)₂]²⁺, as compared to **1**, [Ru(bpy)₂(dppn)]²⁺ (Figure 2a). Similarly, the molar extinction coefficients for **5** are greater than those of **4** in the ultraviolet (UV) and near-UV regions.

Electronic Structure Calculations. DFT and TD-DFT calculations were undertaken on **1**, **3**, and **4**, and were compared to those for [Ru(bpy)₃]²⁺, to gain further insight into the electrochemical and photophysical properties of the cyclometallated complexes. The energies of the frontier molecular orbitals (MOs) and the contributions from the Ru center and the ligands are listed in Tables S1–S2, while the MO diagrams and electron densities of selected MOs are depicted in Figure 3. The energy values were converted to a thermodynamic scale of V vs NHE, with the assumption that 0.0 V vs NHE corresponds to a vacuum level of −4.5 eV.⁴⁹

The HOMO, HOMO-1, and HOMO-2 of the cyclometallated complex **3** are primarily localized on the metal center, with calculated Ru contributions of 56%, 60%, and 74%, respectively (Table S1). A point of interest, however, is the significant contribution to these orbitals from the cyclometallating ligand, including 26% in the HOMO. This covalent bonding from the phpy[−] ligand results in the destabilization of these three occupied orbitals relative to those [Ru(bpy)₃]²⁺, in agreement with the less positive oxidation potential of **3** as compared to that of [Ru(bpy)₃]²⁺, as well as the red shift of the ¹MLCT absorption maximum. The latter is evident from the comparison of the HOMO–LUMO (LUMO = lowest unoccupied molecular orbital) gaps, Δ*E*_{HOMO–LUMO}, among the complexes. The HOMO of **3** is calculated to lie 0.97 eV above that of [Ru(bpy)₃]²⁺, but the energy difference in the LUMOs of the two complexes is smaller (0.36 eV), resulting in a smaller HOMO–LUMO gap in **3** as compared to that of [Ru(bpy)₃]²⁺, with Δ*E*_{HOMO–LUMO} values of 2.81 and 3.41 eV, respectively (Figure 3 and Table S1). It is evident from Table S1 that the LUMO+1, LUMO+2, and LUMO+3 MOs of **3** have contributions from the π* orbitals of the three ligands, but the contribution from bpy is significantly greater than that from phpy[−] in the lower-lying LUMO, LUMO+1, and LUMO+2. The greatest contribution from phpy[−], 67%, is calculated in the LUMO+3, which lies 0.79 eV above the LUMO (Table S1).

Thus, it is expected that the lowest energy ¹MLCT absorption observed in the 450–600 nm range in **3** involves the bpy(π*) MOs, whereas those at higher energies (300–400 nm region) contains Ru(4dπ)→phpy[−](π*) transitions, in agreement with calculations reported by others for the same complex.⁶

It is evident from the data depicted in Figure 3 and Tables S1 and S2 that the HOMO and HOMO-1 of **1** are calculated to lie at very similar energies (within 0.02 eV) and are localized on the electron-rich π-system of the dppn ligand that is distal to the metal center, dppn^{dis}, and the Ru metal, respectively. This result has been reported by us and others for this and related complexes.³² The MOs with metal character in **1** are the HOMO-1 (57%), HOMO-2 (68%) and HOMO-3 (72%), and lie 0.02, 0.18, and 0.20 eV below the dppn^{dis}-based HOMO, respectively. In addition, there is significant dppn^{dis} contribution (23%) to the HOMO-1 (Table S2). These three metal-based occupied MOs are calculated at similar energies as those of the respective orbitals of [Ru(bpy)₃]²⁺. The LUMO, LUMO+3 and LUMO+4 of **1** possess 99%, 65%, and 76% dppn character, respectively, whereas the LUMO+1, LUMO+2 and LUMO+5 are mainly delocalized over the π* orbitals of the bpy ligands (76%, 77%, 88%, respectively). In the latter three MOs, there is also significant contribution from the portion of the dppn ligand that is proximal to the metal center, dppn^{prox}, with 23% and 17% dppn^{prox} character in the LUMO+1 and LUMO+2, respectively (Table S2).

In **4**, the presence of the cyclometallating ligand does not affect the energy of the occupied MO with dppn^{dis} character, and it appears as the HOMO-3 and at nearly the same energy (within 0.1 eV) as the HOMO of [(Ru(bpy)₂(dppn)]²⁺ (Figure 3 and Table S2). However, it is evident from Figure 3 that the presence of the phpy[−] ligand does result in an increase of the energy of the metal-based HOMO, HOMO-1, and HOMO-2, possessing 43%, 70%, and 65%, Ru character, respectively. These three latter orbitals lie 0.85, 0.63, and 0.45 eV above the HOMO-3 in energy, respectively, and are calculated at nearly the same energy (within 0.06 eV) as the respective metal-centered orbitals of **3**, indicating that the replacement of bpy in **3** for dppn in **4** does not affect the energy of the ruthenium-

based MOs. Regarding the unoccupied orbitals in **4**, the LUMO is 99% localized on dppn^{dis}, and the LUMO+2 and LUMO+3 also exhibit significant dppn^{prox} character, 89% and 59%, respectively. The LUMO+1 and LUMO+4 are calculated to be composed of mostly bpy character, 63% and 69%, respectively, with appreciable contribution from dppn^{prox} to the LUMO+1, 31%. The first unoccupied MO with significant phpy⁻ contribution (24%) is the LUMO+4 (3.62 eV above the HOMO), while the LUMO+5 possesses greater phpy⁻ character (76%) as compared to all the unoccupied MOs mentioned above.

The lowest energy singlet excited states, ¹ES₁, of [Ru(bpy)₃]²⁺, **1**, and **3** are ¹MLCT in nature (Tables S3–S5), but the dppn-centered ¹ππ* excited state of **1**, ¹ES₂, is calculated to lie only 96 cm⁻¹ (0.012 eV) above the ¹ES₁ ¹MLCT state (Table S5). This energy difference is very small, and indeed, the ³ππ* excited state was shown experimentally to lie below the ³MLCT in this complex.³² Owing to the higher energy HOMO in **4** as compared to that in **1**, the lowest energy excited state of the former is MLCT in nature, and significant ligand-centered (LC) contribution is not calculated in states below ¹ES₈, with vertical energy 6853 cm⁻¹ (0.85 eV) above ¹ES₁ (Table S6). The absorption spectra of **4** and **5** (Figure 2b) exhibit a tail that extends from 600 to 700 nm. The calculations predict an MLCT transition from the HOMO-1 to the LUMO for **4** at 704 nm, expected to be weaker than that calculated at 544 nm (Table S6). Therefore, the calculations, together with relatively intense absorption ($\epsilon \sim 1000\text{--}5000 \text{ M}^{-1}\text{cm}^{-1}$), can be used to assign the low energy absorption as ¹GS→¹MLCT (Ru→dppn).

The Ru→dppn ¹MLCT state, ¹ES₁, of **1** lies 2000 cm⁻¹ below that of the Ru→bpy ¹MLCT of [Ru(bpy)₃]²⁺ (Tables S3 and S5), as expected from the lower energy dppn π* MO as compared to that of bpy. The Ru→dppn ¹MLCT state, ¹ES₁, of **4** lies 6,251 cm⁻¹ (0.78 eV) below that of **1**, a difference that results primarily from the higher energy HOMO in the former. It should be noted that the difference between the HOMO–LUMO gaps of **1** (2.82 eV) and **4** (2.04 eV), is 0.78 eV (Table S2), consistent with the calculated difference in energy between the ¹ES₁ states of the two complexes (Tables S5 and S6). The lowest energy maxima of **1** and **4** may also be compared, 444 and 546 nm, resulting in an energy difference of 0.52 eV, however, these transitions are expected to correspond to ¹ES₁₁ and ¹ES₆, respectively, based on the calculated intensities (Tables S5 and S6).

Steady-State Emission and Time-Resolved Spectroscopy. The steady-state luminescence and transient absorption spectroscopy of [Ru(bpy)(dppz)₂]²⁺ and **2** parallel those of the corresponding monosubstituted complexes, [Ru(bpy)₂(dppz)]²⁺ and **1**, respectively. The ³MLCT excited state of the PF₆⁻ salt of [Ru(bpy)(dppz)₂]²⁺ is emissive in CH₃CN ($\tau = 720 \text{ ns}$) with maximum at 620 nm ($\lambda_{\text{exc}} = 500 \text{ nm}$). The transient absorption spectrum of [Ru(bpy)(dppz)₂]²⁺ in CH₃CN is consistent with the formation of the vibrationally cooled ³MLCT state within $\sim 20 \text{ ps}$ with positive absorption in the 370–390 nm and 500–600 nm ranges and ground state bleach in the 400–480 nm region, as is typical of related Ru(II) polypyridyl complexes (Figure S12).^{27–29} The intensity of these spectral features do not change from 40 ps to 2 ns and are observed at longer times, where it is evident that they decay monoexponentially to regenerate the ground state with $\tau = 720 \text{ ns}$ ($\lambda_{\text{exc}} = 532 \text{ nm}$, fwhm $\sim 8 \text{ ns}$, Figure S13), indicative that the emission and the observed transient arise

from the same excited state. These photophysical properties are similar in CH₂Cl₂ (Figure S17) and to those previously reported for [Ru(bpy)₂(dppz)]²⁺ and related complexes.^{32,50–52}

In contrast, the cation [Ru(bpy)(dppn)₂]²⁺ (**2**) is not emissive in CH₃CN or H₂O, and its transient absorption spectrum is long-lived, $\tau = 20 \mu\text{s}$, with a maximum in the 520–540 nm range ($\lambda_{\text{exc}} = 532 \text{ nm}$, fwhm $\sim 8 \text{ ns}$, Figure S14), both of which resemble the properties reported for **1** and are consistent with a dppn-centered ³ππ* excited state.³² In addition, the ultrafast transient absorption of **2** shown in Figure S15 is consistent with the formation of the dppn ³ππ* state within 1 ps, and the absorption in the 500 to 550 nm range sharpens resulting in a maximum at 540 nm as it vibrationally cools with a time constant of 10 ps (Figure S15). Similar results were obtained in CH₂Cl₂ (Figure S17). Owing to the long-lived dppn-centered ³ππ* excited state of **2** and its efficient intersystem crossing afforded by the presence of the metal, the quantum yield for the sensitization of ¹O₂, Φ¹O₂, was measured to be 0.98 ($\lambda_{\text{irr}} = 405 \text{ nm}$), similar to that of the efficient DNA photocleavage of **1**.³²

The photophysical results for [Ru(bpy)₃]²⁺, [Ru(bpy)(dppz)₂]²⁺, **1**, and **2** represent a comparison group to the cyclometallated systems **3–5**. The emission of **3** in CH₃CN is observed in the near-infrared region with a maximum at 849 nm (298 K); the excitation spectrum overlays well on the absorption spectrum in the same solvent, indicating that the luminescence stems from the complex and not from a highly emissive impurity. Very weak emission is also observed for **4** and **5** in CH₃CN at 77 K, with maxima at 950 and 935 nm, respectively (Figure S16). A shoulder is discerned for **4** at $\sim 1050 \text{ nm}$, and for **5** at $\sim 1080 \text{ nm}$, which may be ascribed to vibronic progressions in each complex with respective energies of $\sim 1002 \text{ cm}^{-1}$ and $\sim 1436 \text{ cm}^{-1}$, which are consistent with those previously measured in the low-temperature emission spectra of the ³MLCT states of ruthenium polypyridyl complexes.^{54–56} This assignment is also consistent with the energy of the ³ππ* of dppn previously estimated at higher energy ($\sim 1.5 \text{ eV}$, $\sim 826 \text{ nm}$).³²

The transient absorption spectra of **3** in the picosecond ($\lambda_{\text{exc}} = 580 \text{ nm}$, fwhm = 300 fs) and nanosecond ($\lambda_{\text{exc}} = 532 \text{ nm}$, fwhm $\sim 8 \text{ ns}$) timescales are shown in Figure 4. The positive absorption in the 350–380 nm range, with $\tau \sim 9 \text{ ns}$, is consistent with the absorption of the reduced bpy ligand and, therefore, the ³MLCT excited state of the complex. This assignment is consistent with that of related complexes and from calculations, which predict a Ru→bpy lowest energy singlet excited state of **3** (Table S4), assuming the same state ordering in the triplet manifold.

The ultrafast transient absorption spectra of **4** and **5** in CH₃CN are displayed in Figure 5 ($\lambda_{\text{exc}} = 595 \text{ nm}$, fwhm = 300 fs), showing similar spectral features and decays for both complexes. In each case, there is a bleach evident from $\sim 440 \text{ nm}$ to the edge of the spectral window, $\sim 525 \text{ nm}$. Both complexes also exhibit a strong positive transient absorption signal in the 350–440 nm range, superimposed on the bleach signal; the latter results in apparent vibronic structure because of the sharp dppn ¹ππ* absorption peaks observed in the ground state spectra of **4** and **5** (Figure 2b). An important point of the observed signal is the absence of the strong, long-lived absorption in the 470–650 nm range known to correspond to the dppn-centered ³ππ* state previously reported in the free ligand and **1**,³² and observed here for **2** (Figures S14 and S15). Since the energies of the dppn-centered

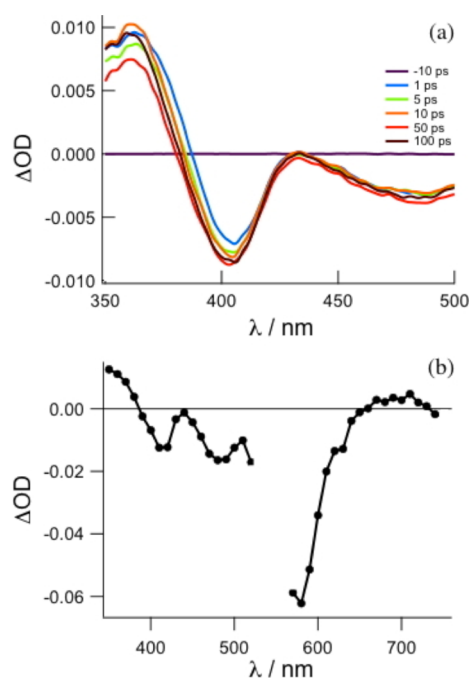


Figure 4. Transient absorption spectra of **3** in CH_3CN at (a) 1 to 100 ps following a 580 nm excitation (fwhm = 300 fs, 1.0 mM) and (b) 1 ns after a 532 nm pulse (fwhm \sim 8 ns, 71 μM).

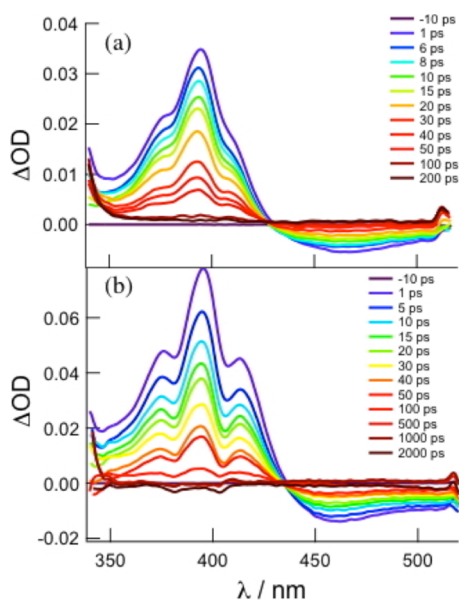


Figure 5. Transient absorption spectra of (a) 0.96 mM **4** and (b) 0.70 mM **5** in CH_3CN at several delay times following a 595 nm excitation pulse (fwhm = 300 fs).

MOs are not affected by cyclometallation, the position of this peak is not expected to shift in **4** and **5** compared to **1** and **2**. Instead, a strong positive signal is observed from 350 to 420 nm, consistent with the absorption of reduced bpy, phen, and related ligands in the $^3\text{MLCT}$ excited states of related complexes.^{29,50–52,54}

The $^3\text{MLCT}$ state absorption of **4** at 395 nm and the bleach at 470 nm can be fitted to monoexponential decays with $\tau = 25$ ps. The signal at 395 nm of **5** decays biexponentially with $\tau_1 = 8(1)$ ps and $\tau_2 = 45(1)$ ps. Similar kinetics are observed for the bleach signal at 460 nm, with lifetimes of ~ 10 ps and ~ 50 ps;

these lifetimes are approximate because the signal is too weak to obtain good fits. Since there are no spectral changes from 1 to 500 ps (Figure 5b), the observed transient must be associated with a single excited state, the $^3\text{MLCT}$. The 8 ps component may be ascribed to vibrational cooling after the initial population of the $^3\text{MLCT}$ state, followed by the 45 ps decay to regenerate the ground state. A 2 nm blue-shift is observed for the 395 nm peak of **5** from 1 to 5 ps, consistent with vibrational cooling within the $^3\text{MLCT}$ state. Similar small shifts and absence of sharpening has been observed by us and others for related Ru(II) complexes, with vibrational cooling times that typically range from 2 to 20 ps.^{27,53,57–59} This timescale for vibrational cooling is supported by time-resolved vibrational techniques for ruthenium(II) and rhenium(I) complexes.^{60,61} It is not clear why a similar vibrational cooling component is not present in **4**; however, it is possible that because of the shorter excited state lifetime, both vibrational cooling in the $^3\text{MLCT}$ state and decay to the ground state take place in the same timescale such that the two processes cannot be resolved.

The short lifetimes and spectral profiles of **4** and **5** are inconsistent with the long-lived dppn $^3\pi\pi^*$ excited state observed in **1** and **2** ($\tau \sim 20 \mu\text{s}$), and may be explained by the low energy of Ru→dppn $^3\text{MLCT}$ excited states in **4** and **5** as compared to the Ru→bpy $^3\text{MLCT}$ in **3**. In CH_2Cl_2 , similar spectral profiles are observed for **4** and **5**, with lifetimes of 150 and 220 ps, respectively (Figure S18). The relatively fast nonradiative deactivation in **4** and **5** can be attributed to the smaller energy difference between the $^3\text{MLCT}$ and the ground states in these complexes as compared to **3**.⁶² The longer lifetimes measured in CH_2Cl_2 as compared to CH_3CN are consistent with this explanation, since the $^3\text{MLCT}$ states of the complexes are expected to lie at higher energy in the nonpolar solvent. It should also be noted that the energy of the dd states, which are typically involved in deactivation of the $^3\text{MLCT}$ states of ruthenium polypyridyl complexes, are expected to lie at similar energies in **3** – **5**. Therefore, the shorter lifetimes of **4** and **5** as compared to **3** cannot be explained by changes in the energies of the ligand field states. The weak emission in the near-IR observed for **4** and **5** at 77 K ($\lambda_{\text{exc}} = 405$ nm, 5 mW) is also consistent with the short lifetime of the excited states of these complexes.

The energies of the lowest triplet states of **1** and **2** are compared to the corresponding cyclometallated complexes **4** and **5** in Figure 6, as well as those of the parent compounds $[\text{Ru}(\text{bpy})_3]^{2+}$ and **3**. Although the dppn $^3\pi\pi^*$ state (~ 1.5 eV) is lower in energy than the Ru-dppn $^3\text{MLCT}$ states in **1** and **2**, the

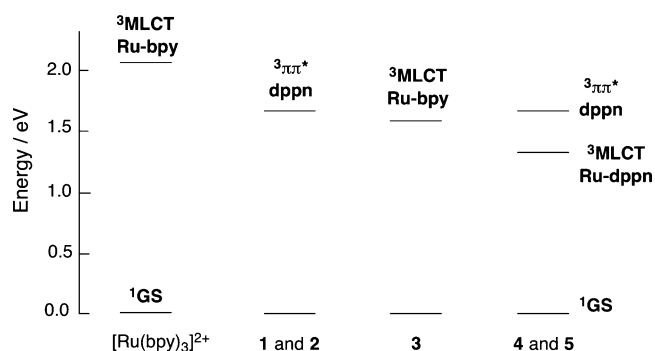


Figure 6. Relative energies of the low-lying triplet states of selected complexes.

higher energy Ru-based HOMO in **4** and **5** results in a low-energy $^3\text{MLCT}$ state (at ~ 1.3 eV based on the energy of the 77 K emission). In the latter case, it is expected that the energy of the $^3\pi\pi^*$ states is similar to those in **1** and **2**, since the dppn-centered MOs remain relatively unaffected by cyclometallation. This is also evident experimentally in the absorption spectra of the complexes, where there is little shift in the energies of the $^1\pi\pi^*$ transitions among **1**, **2**, **4**, and **5** (Table 1 and Figure 2).

CONCLUSIONS

The present work reports the preparation, characterization, and photophysical properties of new cyclometallated Ru(II) complexes equipped with the phpy^- ligand. These systems are compared to their bpy analogs. Unlike **1** and **2**, with long-lived dppn-centered $^3\pi\pi^*$ excited states ($\tau \sim 20$ μs), the corresponding cyclometallated complexes $[\text{Ru}(\text{phpy})(\text{bpy})(\text{dppn})]^+$ (**4**) and $[\text{Ru}(\text{phpy})(\text{dppn})_2]^+$ (**5**) exhibit Ru \rightarrow dppn $^3\text{MLCT}$ states with lifetimes of 25 and 45 ps, respectively. Although it is desirable to shift the absorption of ruthenium dyes used in DSSCs to lower energies, it is evident from this work that, for cyclometallated phpy^- complexes, lowering the energy of the $^3\text{MLCT}$ state below that of $[\text{Ru}(\text{phpy})(\text{bpy})_2]^+$ results in significant shortening of the excited state lifetime. If the $^3\text{MLCT}$ excited state decay competes with charge injection, it will result in a decrease in efficiency of the device. Moreover, a smaller driving force is expected for charge injection from the $^1\text{MLCT}$ state, as previously reported for other systems, since this state now lies at lower energy.

ASSOCIATED CONTENT

Supporting Information

NMR spectra and resonance assignments, electrochemistry, calculations, additional transient absorption spectra, and low temperature emission. These materials are available free of charge via the Internet at <http://pubs.acs.org>.

AUTHOR INFORMATION

Corresponding Author

*E-mail: turro@chemistry.ohio-state.edu.

Notes

The authors declare no competing financial interest.

ACKNOWLEDGMENTS

C.T. and K.R.D. thank the National Science Foundation (CHE 1213646) for support of this work, and B.P. thanks the Texas Higher Education Coordinating Board for support through the Good Neighbor Scholarship. K.R.D. thanks the Laboratory for Molecular Simulation at Texas A&M University for providing software, support, and computer time (NSF CHE-0541587). C.T. thanks the Ohio Supercomputer Center and the Center for Chemical and Biophysical Dynamics (CCBD) at OSU.

REFERENCES

- (1) Bomben, P. G.; Robson, K. C. D.; Koivisto, B. D.; Berlinguette, C. P. *Coord. Chem. Rev.* **2012**, *256*, 1438–1450.
- (2) Koivisto, B. D.; Robson, K. C. D.; Berlinguette, C. P. *Inorg. Chem.* **2009**, *48*, 9644–9652.
- (3) Robson, K. C. D.; Koivisto, B. D.; Yella, A.; Spornova, B.; Nazeeruddin, M. K.; Baumgartner, T.; Grätzel, M.; Berlinguette, C. P. *Inorg. Chem.* **2011**, *50*, 5494–5508.
- (4) Bomben, P. G.; Thériault, K. D.; Berlinguette, C. P. *Eur. J. Inorg. Chem.* **2011**, 1806–1814.
- (5) Bomben, P. G.; Gordon, T. J.; Schott, E.; Berlinguette, C. P. *Angew. Chem., Int. Ed.* **2011**, *50*, 10682–10685.
- (6) Bomben, P. G.; Robson, K. C. D.; Sedach, P. A.; Berlinguette, C. P. *Inorg. Chem.* **2009**, *48*, 9631–9643.
- (7) Bessho, T.; Yoneda, E.; Yum, J.-H.; Guglielmi, M.; Tavernelli, I.; Iami, H.; Rothlisberger, U.; Nazeeruddin, M. K.; Grätzel, M. *J. Am. Chem. Soc.* **2009**, *131*, 5930–5934.
- (8) Wadman, S. H.; Kroon, J. M.; Bakker, K.; Havenith, R. W. A.; van Klink, G. P. M.; van Koten, G. *Organometallics* **2010**, *29*, 1569–1579.
- (9) Kim, J.-J.; Choi, H.; Paek, S.; Kim, C.; Lim, K.; Ju, M.-J.; Kang, H. S.; Kang, M.-S.; Ko, J. *Inorg. Chem.* **2011**, *50*, 11340–11347.
- (10) Kisserwan, H.; Ghaddar, T. H. *Dalton Trans.* **2011**, *40*, 3877–3884.
- (11) Cline, E. D.; Bernhard, S. *Chimia* **2009**, *63*, 709–713.
- (12) Baranoff, E.; Yum, J.-H.; Grätzel, M.; Nazeeruddin, M. K. *J. Organomet. Chem.* **2009**, *694*, 2661–2670.
- (13) Williams, J. A. G.; Wilkinson, A. J.; Whittle, V. L. *Dalton Trans.* **2008**, *16*, 2081–2099.
- (14) Jensen, R. A.; Van Ryswyk, H.; She, C.; Szarko, J. M.; Chen, L. X.; Hupp, J. T. *Langmuir* **2010**, *26*, 1401–1404.
- (15) She, C.; Guo, J.; Irle, S.; Morokuma, K.; Mohler, D. L.; Zabari, H.; Odobel, F.; Youm, K.-T.; Liu, F.; Hupp, J. T.; Lian, T. *J. Phys. Chem. A* **2007**, *111*, 6832–6842.
- (16) Koops, S. E.; O'Regan, B. C.; Barnes, P. R. F.; Durrant, J. R. *J. Am. Chem. Soc.* **2009**, *131*, 4808–4818.
- (17) Haque, S. A.; Palomares, E.; Cho, B. M.; Green, A. N. M.; Hirata, N.; Klug, D. R.; Durrant, J. R. *J. Am. Chem. Soc.* **2005**, *127*, 3456–3462.
- (18) Imahori, H.; Kang, S.; Hayashi, H.; Haruta, M.; Kurata, H.; Isoda, S.; Canton, S. E.; Inafahsaeng, Y.; Kathiravan, A.; Pascher, T.; Chábera, Yartsev, A. P.; Sundström, V. *J. Phys. Chem. A* **2011**, *115*, 3679–3690.
- (19) Nemect, H.; Rochford, J.; Tratula, O.; Gloppini, E.; Kuzel, P.; Polivka, T. J.; Yartsev, A. P.; Sundström, V. *J. Phys. Rev. Lett.* **2010**, *104*, 197401.
- (20) Myllyperkiö, P.; Benkö, G.; Korppi-Tommola, J.; Yartsev, A. P.; Sundström, V. *J. Phys. Chem. Chem. Phys.* **2008**, *10*, 996–1002.
- (21) Pan, Jie; Benkö, G.; Xu, Y.; Pascher, T.; Sun, L.; Sundström, V.; Polivka, T. *J. Am. Chem. Soc.* **2002**, *124*, 13949–13957.
- (22) Watson, D. F.; Meyer, G. J. *Annu. Rev. Phys. Chem.* **2005**, *56*, 119–156.
- (23) Listorti, A.; O'Regan, B.; Durrant, J. R. *Chem. Mater.* **2011**, *23*, 3381–3399.
- (24) Qu, P.; Thomson, D. W.; Meyer, G. J. *Langmuir* **2000**, *16*, 4662–4671.
- (25) Ardo, S.; Meyer, G. J. *Chem. Soc. Rev.* **2009**, *38*, 115–164.
- (26) Anderson, N. A.; Lian, T. *Annu. Rev. Phys. Chem.* **2005**, *56*, 491–519.
- (27) Liu, Y.; Turner, D. B.; Singh, T. N.; Angeles-Boza, A. M.; Chouai, A.; Dunbar, K. R.; Turro, C. J. *Am. Chem. Soc.* **2009**, *131*, 26–27.
- (28) Bhasikuttan, A. C.; Suzuki, M.; Nakashima, S.; Okada, T. *J. Am. Chem. Soc.* **2002**, *124*, 8398–8405.
- (29) McCusker, J. K. *Acc. Chem. Res.* **2003**, *36*, 876.
- (30) Cannizzo, A.; van Murik, F.; Gawelda, W.; Zgrablic, G.; Bressler, C.; Ghergui, M. *Angew. Chem., Int. Ed.* **2006**, *45*, 3174–3176.
- (31) Yoon, S.; Kukura, P.; Stuart, C. M.; Mathies, R. A. *Mol. Phys.* **2006**, *104*, 1275–1282.
- (32) Sun, Y.; Joyce, L. E.; N. M.; Dickson, N. M.; Turro, C. *Chem. Commun.* **2010**, *46*, 2426–2428.
- (33) Sun, Y.; El Ojaimi, M.; Hammitt, R.; Thummel, R. P.; Turro, C. *J. Phys. Chem. B* **2010**, *114*, 14664–14670.
- (34) Liu, Y.; Hammitt, R.; Lutterman, D. A.; Joyce, L. E.; Thummel, R. P.; Turro, C. *Inorg. Chem.* **2009**, *48*, 375–385.
- (35) Polson, M.; Chiorboli, C.; Fracasso, S.; Scandola, F. *Photochem. Photobiol. Sci.* **2007**, *6*, 438–443.
- (36) Johansson, P. G.; Rowley, J. G.; Taheri, A.; Meyer, G. J. *Langmuir* **2011**, *27*, 14522–14531.

- (37) Petroni, A.; Slep, L. D.; Etchenique, R. *Inorg. Chem.* **2008**, *47*, 951–956.
- (38) Fernandez, S.; Pfeffer, M.; Ritleng, V.; Sirlin, C. *Organometallics* **1999**, *18*, 2390–2394.
- (39) Ryabov, A. D.; Lagadec, R. L.; Estevez, H.; Toscano, R. A.; Hernandez, S.; Alexandrova, L.; Kurova, V. S.; Fischer, A.; Sirlin, C.; Pfeffer, M. *Inorg. Chem.* **2005**, *44*, 1626–1634.
- (40) Che, G.; Li, W.; Kong, Z.; Su, Z.; Chu, B.; Li, B.; Zhang, Z.; Hu, Z.; Chi, H. *Synth. Commun.* **2006**, *36*, 2519–2524.
- (41) Foxon, S. P.; Green, C.; Walker, M. G.; Wragg, A.; Adams, H.; Weinstein, J. A.; Parker, S. C.; Meijer, A. J. H. M.; Thomas, J. A. *Inorg. Chem.* **2012**, *51*, 463–471.
- (42) Burdzinski, G.; Hackett, J. C.; Wang, J.; Gustafson, T. L.; Hadad, C. M.; Platz, M. S. *J. Am. Chem. Soc.* **2006**, *128*, 13402–13411.
- (43) Nakayama, T.; Amijima, Y.; Ibuki, K.; Hamanoue, K. *Rev. Sci. Instrum.* **1997**, *68*, 4364–4371.
- (44) Frisch, M. J.; Trucks, G. W.; Schlegel, H. B.; Scuseria, G. E.; Robb, M. A.; Cheeseman, J. R.; Scalmani, G.; Barone, V.; Mennucci, B.; Petersson, G. A. et al. *Gaussian 09*, revision A.02; Gaussian Inc.: Wallingford, CT, 2009. (Full author list can be found in the Supporting Information.)
- (45) Lee, C.; Yang, W.; Parr, R. G. *Phys. Rev. B* **1988**, *37*, 785–789.
- (46) Becke, A. D. *J. Chem. Phys.* **1993**, *98*, 5648–5652.
- (47) Chemissian v2.2 2001: An analyzing tool of molecules electronic structure and spectra. <http://chemissian.com>.
- (48) Sun, Y.; Lutterman, D. A.; Turro, C. *Inorg. Chem.* **2008**, *47*, 6427–6434.
- (49) Grätzel, M. *Nature* **2001**, *414*, 338–344.
- (50) Kuhnt, C.; Karnahl, M.; Tschielei, S.; Griebenow, K.; Schmitt, M.; Schäfer, B.; Kriek, S.; Görls, H.; Rau, S.; Dietzek, B.; Popp, J. *Phys. Chem. Chem. Phys.* **2010**, *12*, 1357–1368.
- (51) Tschielei, S.; Karnahl, M.; Rau, S.; Bietzek, B.; Schmitt, M.; Popp, J. *J. Raman Spectrosc.* **2010**, *41*, 922–932.
- (52) Foxon, S. P.; Alamiry, M. A. H.; Walker, M. G.; Meijer, A. J. H. M.; Sazanovich, I. V.; Winstein, J. A.; Thomas, J. A. *J. Phys. Chem. A* **2009**, *113*, 12754–12762.
- (53) Sun, Y.; Liu, Y.; Turro, C. *J. Am. Chem. Soc.* **2010**, *132*, 5594–5595.
- (54) Juris, A.; Balzani, V.; Barigelletti, F.; Campagna, S.; Belser, P.; von Zelewsky, A. *Coord. Chem. Rev.* **1988**, *84*, 85–277.
- (55) Klassen, D. M.; Crosby, G. A. *J. Chem. Phys.* **1968**, *48*, 1853–1858.
- (56) Sun, Y.; Collins, S. N.; Joyce, L. E.; Turro, C. *Inorg. Chem.* **2010**, *49*, 4257–4262.
- (57) McFarland, S. A.; Cheng, K. W. Y.; Lee, F. S.; Cozens, F. L.; Schepp, N. P. *Can. J. Chem.* **2008**, *86*, 1118–1125.
- (58) Damrauer, N. H.; McCusker, J. K. *J. Phys. Chem. A* **1999**, *103*, 8440–8446.
- (59) Henrich, J. D.; Zhang, H.; Dutta, P. K.; Kohler, B. *J. Phys. Chem. B* **2010**, *114*, 14679.
- (60) Liard, D. J.; Busby, M.; Maousek, P.; Towrie, M.; Vlcek, A., Jr. *J. Phys. Chem. A* **2004**, *108*, 2363–2369.
- (61) Henry, W.; Coates, C. G.; Brady, C.; Ronayne, K. L.; Matousek, P.; Towrie, M.; Botchway, S. W.; Parker, A. W.; Vos, J. G.; Browne, W. R.; McGarvey, J. J. *J. Phys. Chem. A* **2008**, *112*, 4537–4544.
- (62) Caspar, J. V.; Meyer, T. J. *Inorg. Chem.* **1983**, *22*, 2444–2453.